Differential Formation and Circulation of North Pacific Central Mode Water

EITAROU OKA

Institute of Observational Research for Global Change, JAMSTEC, Yokosuka, Japan

TOSHIO SUGA

Institute of Observational Research for Global Change, JAMSTEC, Yokosuka, and Department of Geophysics, Graduate School of Science, Tohoku University, Sendai, Japan

(Manuscript received 23 July 2004, in final form 4 May 2005)

ABSTRACT

A repeat hydrographic section along 165°E was analyzed to verify a westward extension of the formation region of the North Pacific Ocean Central Mode Water (CMW) suggested by previous synoptic observations, and to investigate the relation between the formation region and thermohaline fronts. The CMW formation region extends at least as far west as 155°E, much farther than recognized in a previous study based on climatology. It is located in two interfrontal regions between the Kuroshio Extension front and the Kuroshio Bifurcation front (KBF), and between the KBF and the subarctic front, where two types of CMW—namely, the lighter variety with potential density of 25.8–26.2 kg m^{-3} and the denser one of 26.3–26.4 kg m^{-3}—are formed. How this differential formation of CMW is reflected in its gyrewide distribution was examined using one-time sections of the World Ocean Circulation Experiment (WOCE) Hydrographic Program in the North Pacific. The main circulation paths of the two types of CMW diverge east of the date line; the lighter variety is located in the inner part of the eastern subtropical gyre, and the denser variety is located in the outer part. These results demonstrate that the frontal structure around the northern boundary of the subtropical gyre, particularly the existence of KBF, is essential in determining the properties and the gyrewide distribution of CMW.

1. Introduction

The North Pacific Ocean Central Mode Water (CMW) is characterized by a pycnostad of σ_θ = 26.0–26.5 kg m^{-3} (σ_θ is potential density; Nakamura 1996), or a thermostad with a core temperature of 10°–13°C (Suga et al. 1997), thus identified by its low potential vorticity (PV), lying in the lower ventilated pycnocline, mainly in the central part of the subtropical gyre (Fig. 1). It is formed in late winter in the deep mixed layer near the northern boundary of the gyre and spreads through advection by the clockwise gyral circulation.

Suga et al. (1997) analyzed the climatology of upper thermal fields and inferred that CMW is formed between 175°E and 160°W. However, other studies have presented examples of synoptic observations suggesting that CMW is also formed farther west: at 40°N, 154°E in April 1971 (Nakamura 1996); at 37°N, 165°E in May 1993 (Kawabe and Taira 1998); and at 37°N between 151° and 165°E in February and March 2003 (Oka and Suga 2003). If these examples are not exceptional, the CMW formation region extends much farther westward (upstream) than is recognized in the climatology of Suga et al. (1997). To verify this westward extension, we need to examine a number of synoptic observations west of 175°E near the northern boundary of the subtropical gyre.

Along this northern gyre boundary there are three thermohaline fronts: the Kuroshio Extension front (KEF), the Kuroshio Bifurcation front (KBF), and the subarctic front (SAF), from south to north. Here, the term SAF is used for a boundary between the warmer, saltier water in the subtropical gyre, and the colder, fresher water in the subarctic gyre, characterized by large horizontal gradients of temperature and salinity at depths less than 100 dbar (Roden 1970, 1972; Zhang and Hanawa 1993; Yuan and Talley 1996). Nakamura

Corresponding author address: Dr. Eitarou Oka, Institute of Observational Research for Global Change, JAMSTEC, 2-15 Natsushima-Cho, Yokosuka, Kanagawa 237-0061, Japan.
E-mail: okae@jamstec.go.jp

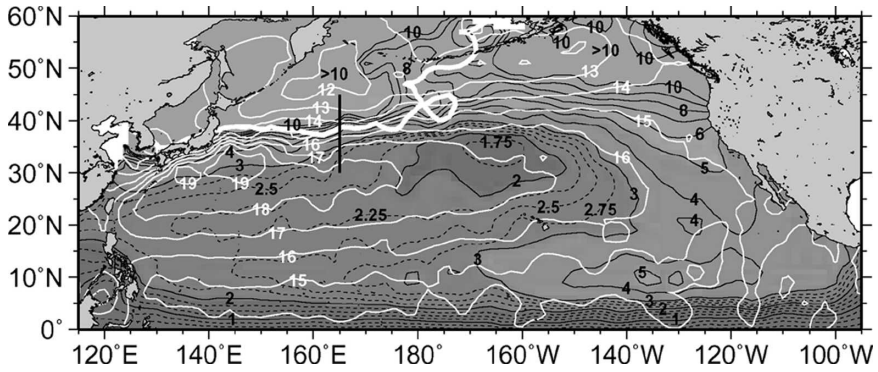

FIG. 1. Annual-mean climatology of PV (10^{-10} m^{-1} s^{-1}; thin black contours with shade) and pressure anomaly streamfunction (m^2 s^{-2}; thin white contours) relative to 2000 dbar on the isopycnal of σ_θ = 26.2 kg m^{-3}, adapted from Suga et al. (2004). The thick white contour denotes the winter outcrop of the isopycnal. The thick black line denotes the part of the 165°E section used in this study.

(1996) inferred that CMW is formed between the SAF and the "9°C front" at 300-m depth, which represents, by his definition, a branch of the main path of the Kuroshio Extension rather than the KBF. Suga et al. (1997) mentioned that CMW is formed between the KEF and the KBF, although they did not examine the region north of the KBF because of a lack of salinity data. Both of these studies described the formation region in relation to the frontal structure but were based on climatologies in which fronts with high temporal and spatial variability are not adequately depicted. To clarify the relation between the CMW formation region and the fronts, an examination of synoptic sections across them is crucial.

Kawabe and Taira (1998), analyzing the World Ocean Circulation Experiment (WOCE) Hydrographic Program (WHP) P13J section along 165°E in May 1993, indicated that CMW is formed between the KEF and the KBF, which agrees with the inference of Suga et al. (1997). Furthermore, a recent numerical simulation by Tsujino and Yasuda (2004) demonstrated that CMW is formed both between the KEF and the KBF, and between the KBF and the SAF, with different densities across the KBF. These results need to be verified by analyzing more synoptic sections across the fronts.

The Japan Meteorological Agency (JMA) has repeated hydrographic and chemical observations at a section along 165°E (Fig. 1) a couple of times per year since 1996 to quantitatively understand oceanic variations and greenhouse gas circulations in the western North and equatorial Pacific that are closely related to climate variations. This paper analyzes this repeat section in 1996–2003, supplemented by three WHP one-time sections along 165°E in 1991–93, to verify the possible westward extension of the CMW formation region and to investigate the relation between the formation region and the fronts. Since the mean flow at this section is predominantly eastward, the CMW appearing there is believed to be formed to the west. Therefore, constant existence of the CMW in the section will verify that the CMW formation region extends at least as far west as 165°E. We will also clarify that CMW is formed in the two interfrontal regions between the KEF and the KBF and between the KBF and the SAF and that the CMW formed in the southern interfrontal region is significantly warmer and lighter than that formed in the northern region, which agrees with the numerical result of Tsujino and Yasuda (2004). How this differential formation of CMW is reflected in its gyrewide distribution is further investigated using the WHP one-time sections in the North Pacific.

The data used are explained in section 2. The locations of the fronts at the 165°E section are determined in section 3. In section 4, the CMW appearing in the 165°E section is examined in detail, focusing on the time and the locations of its formation. The gyrewide distribution of the two types of CMW is studied in section 5. Summary and discussion are given in section 6.

2. Data

Temperature and salinity data of the 165°E section between 30° and 45°N in springs of 1996–98 and 2000–03, and summers of 1996–98, obtained by the JMA (1997, 1998, 1999, 2001, 2002, 2003), were used (Table 1). The data from spring 1999 were not used because the observations were limited to the north of 40°N, covering only a small portion of the CMW distribution range. The observations were conducted at intervals of 1° latitude using a conductivity–temperature–depth

TABLE 1. Latitudes and dates of the observations at 165°E in (a) spring and (b) summer, used in this study. Latitudes of the KEF, KBF, and SAF at 165°E are also presented.

(a)

Year	Lat (°N)	Date	KEF (°N)	KBF (°N)	SAF (°N)
1993	30–45	18–25 May	33–34	37–39	39–41
1996	32–45	19–24 May	31–32	37–38	40–41
1997	30–45	07–11 Jun	34–35	37–38	40–41
1998	30–45	17–21 Jun	35–37	39–40	41–42
2000	30–45	09–14 May	33–34	37–39	40–41
2001	35–45	16–19 May	33–35	37–38	40–41, 42–43
2002	30–45	18–22 May	36–37	38–40	41–42
2003	37–45	03–06 May	No data	37–39	40–42

(b)

Year	Lat (°N)	Date	KEF (°N)	KBF (°N)	SAF (°N)
1991	30–40	17–22 Aug	34–35	38–39	No data
1992	30.7–45	30 Aug–10 Sep	34–34.7	38.5–39.5	41.5–42
1996	30–45	14–19 Oct	35–36	37–38	40–42
1997	30–45	18–22 Sep	33–34	37–38	41–42
1998	30–45	23–27 Sep	35–36	—	41–42

profiler (CTD), except at 34°N in spring 1998, where an expendable CTD (XCTD) was used, and at 40° and 41°N in summer 1996 and 41°–45°N in summer 1998, where an expendable bathythermograph (XBT) was used.

The temperature and salinity data at every 1 dbar were vertically smoothed using a seven-point median filter, and then a three-point Hanning filter with weights of 0.25, 0.5, and 0.25, 10 times. From these data, potential temperature and density referred to the surface were calculated. Assuming that relative vorticity is negligible, PV was calculated from

$$\mathrm{PV} = -\frac{f}{\rho}\frac{\partial \rho_\theta}{\partial z}, \tag{1}$$

where f is the Coriolis parameter, ρ is in situ density, ρ_θ potential density, and z is the upward coordinate.

Dissolved oxygen was measured at 85% of the hydrographic stations by Niskin bottle sampling at about 20 standard depths, typically at an interval of 25 dbar at depths less than 150 dbar, an interval of 50 dbar at 150–300 dbar, and an interval of 100 dbar or more in the deeper layer. From the dissolved oxygen data, apparent oxygen utilization (AOU), which is the difference between saturated and observed concentrations of dissolved oxygen, was calculated for each standard depth and then interpolated on a 1-dbar grid using the Akima spline (Akima 1970). The AOU of a water parcel tends to increase because of the oxygen consumption through remineralization of organic matter after the water parcel is isolated from the atmosphere. This is used in section 4 to estimate the ages of CMW parcels.

CTD and dissolved oxygen data at three WHP one-time sections along 165°E, named P13, P13C, and P13J, were also used. The P13J section occupied in May 1993 was supplemented as a spring section; P13C in August 1991 and P13 in August–September 1992 were added as summer sections (Table 1). The data from these sections between 30° and 45°N, obtained at intervals of 0.5°–2° latitude, were downloaded from the WHP office Web site (see online at http://whpo.ucsd.edu) and processed in the same way as the JMA data.

3. Thermohaline fronts at the 165°E section

The locations of the KEF, KBF, and SAF at the 165°E section in each observation period were determined (Table 1), from the temperature and salinity distributions (Figs. 2 and 3, left panels), and the following definitions. The SAF is defined as the southward salinity gradient maximum at 100-dbar depth around isohalines of 33.5 to 34.0, based on inspections of salinity sections around 165°E presented in previous studies (Roden 1972; Zhang and Hanawa 1993; Yuan and Talley 1996; Kawabe and Taira 1998). The KEF is defined as the southward temperature gradient maximum at 300 dbar across the 12°C isotherm because the Kuroshio Extension is generally represented by this isotherm at that depth (Mizuno and White 1983). The KBF is defined as the southward temperature gradient maximum at 300 dbar between the KEF and the SAF (Levine and White 1983; Mizuno and White 1983). Locations of the KEF in springs of 1996 and 2001 were beyond the observation range and were estimated using the surface velocity fields of Uchida and Imawaki (2003) as the latitude of the eastward meandering jet of the Kuroshio Extension at 165°E.

In each period, the three fronts are located at intervals of a few degrees latitude (Table 1). The KBF exists in most of the periods but is not distinguished in summer 1998. The SAF separates into two fronts in spring 2001. This is consistent with Yuan and Talley (1996), who mentioned that in the western North Pacific this front is usually a single front but is occasionally divided into two parts.

4. CMW in the 165°E section

a. CMW pycnostads in the 165°E section

In the 165°E section for each observation period, several areas of low PV—namely, pycnostads—are ob-

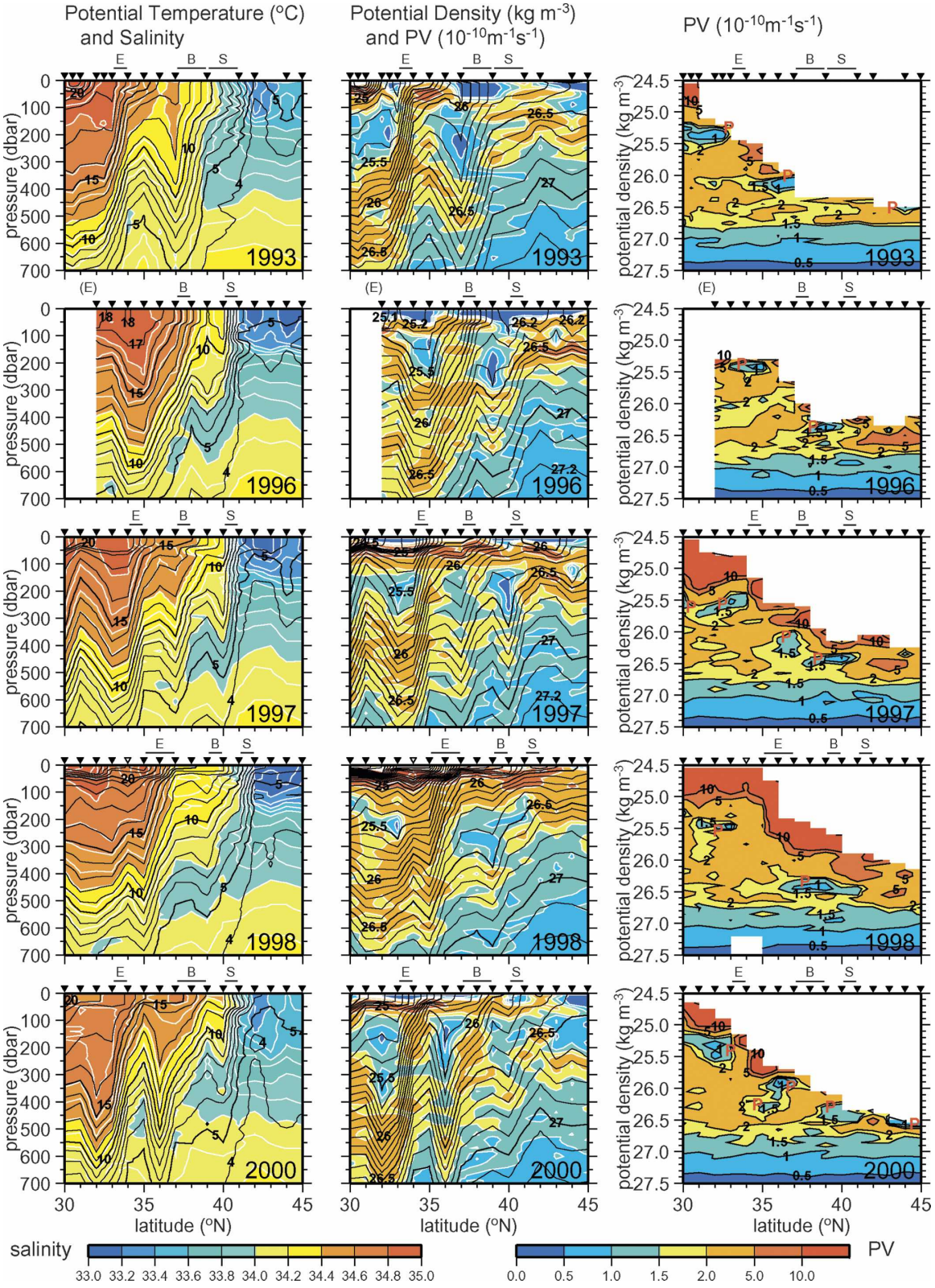

FIG. 2. Distributions of (left) potential temperature (black contours) and salinity (white contours with color), (middle) potential density (black contours) and PV (white contours with color), and (right) PV with respect to potential density at 165°E in spring. Contours for PV are drawn at 0.5, 1, 1.5, 2, 5, and 10×10^{-10} m^{-1} s^{-1}. Black (white) inverted triangles on the top of each panel indicate locations of hydrographic stations with (without) dissolved oxygen measurements, and horizontal bars with "E," "B," and "S" indicate locations of the KEF, KBF, and SAF. A red "P" in the right panels denotes pycnostads examined in this study.

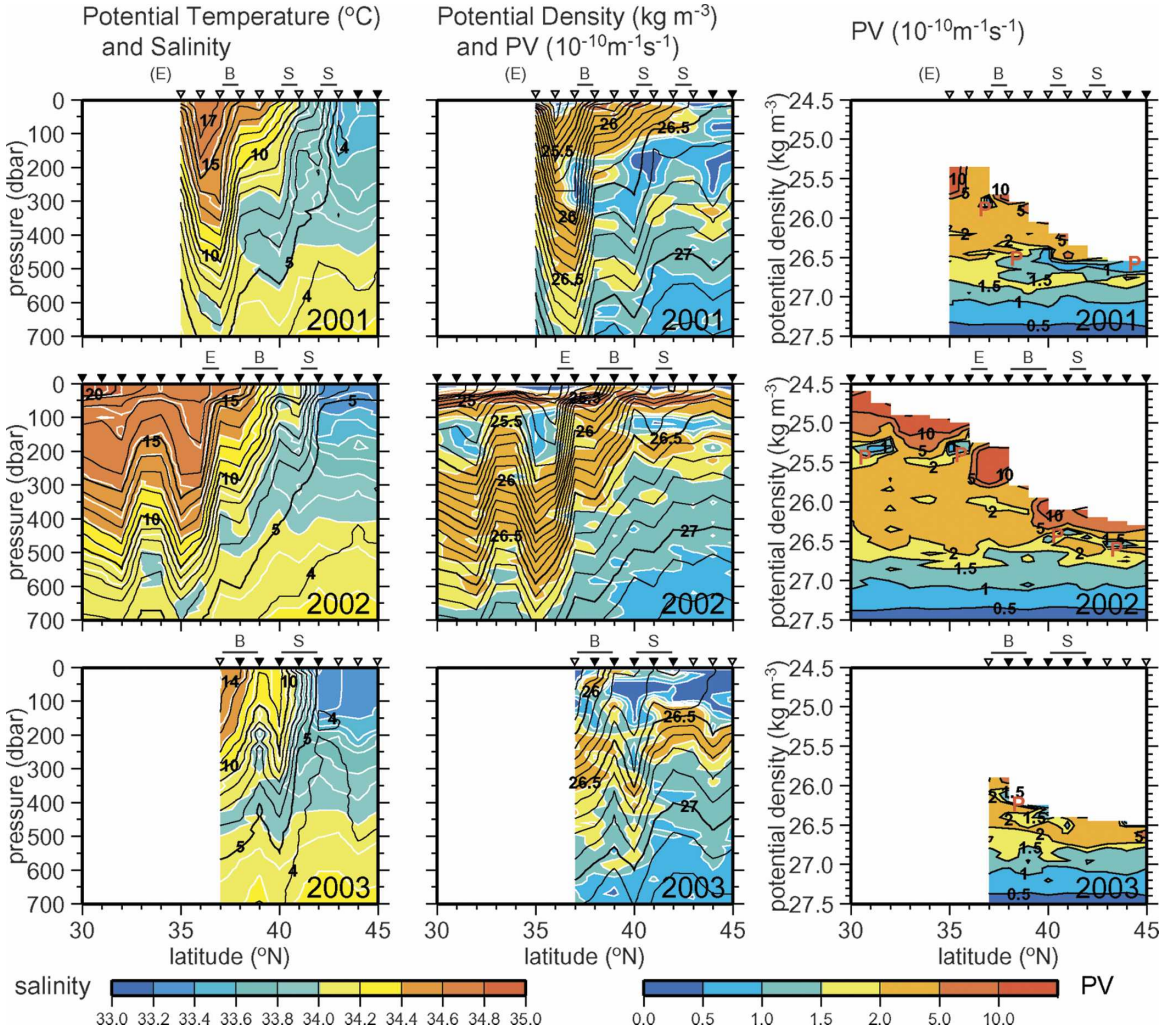

FIG. 2. (*Continued*)

served above the deep, low-PV layer at σ_θ = 26.8 kg m^{-3} and greater (Figs. 2 and 3, middle and right panels). In this study, we define a pycnostad as an area of PV lower than 1.5 × 10^{-10} m^{-1} s^{-1} above the deep, low-PV layer, and treat only those pycnostads that extend for two or more successive stations with a thickness greater than 50 dbar, or that exist at a station with a thickness greater than 100 dbar, neglecting smaller-scale features. Each area of low PV extending for multiple stations is regarded as one pycnostad. In the spring (summer) sections for 8 (5) yr, a total of 24 (14) such "significant" pycnostads are recognized.

In spring, seven pycnostads are located south of the KEF, 13 are located between the KEF and the SAF, and four are located north of the SAF (Fig. 2). Based on the properties (Fig. 4a and Table 2a), the pycnostads south of the KEF are identified as the North Pacific Subtropical Mode Water (STMW) (Masuzawa 1969, 1972), which prevails in the western part of the subtropical gyre, with a density of 24.8–25.7 kg m^{-3} (Suga et al. 2004). The pycnostads between the KEF and the SAF, except for one at 33°–35°N in 1996 with the properties of STMW, are identified as CMW, which is characterized by a density of 25.9–26.5 kg m^{-3} (Nakamura 1996; Suga et al. 2004) or a core temperature of 10°–13°C (Suga et al. 1997). The pycnostads north of the SAF have cold, fresh properties that are characteristic of the subarctic region and are clearly different from CMW. They may be a type of mode water prevailing in the subarctic region of the North Pacific.

In summer, six pycnostads are located south of the KEF, seven are located between the KEF and the SAF, and one is located north of the SAF (Fig. 3). Five of the six pycnostads south of the KEF are STMW, while the other is considered to be CMW (Fig. 4b and Table 2b). Six of the seven between the KEF and the SAF are

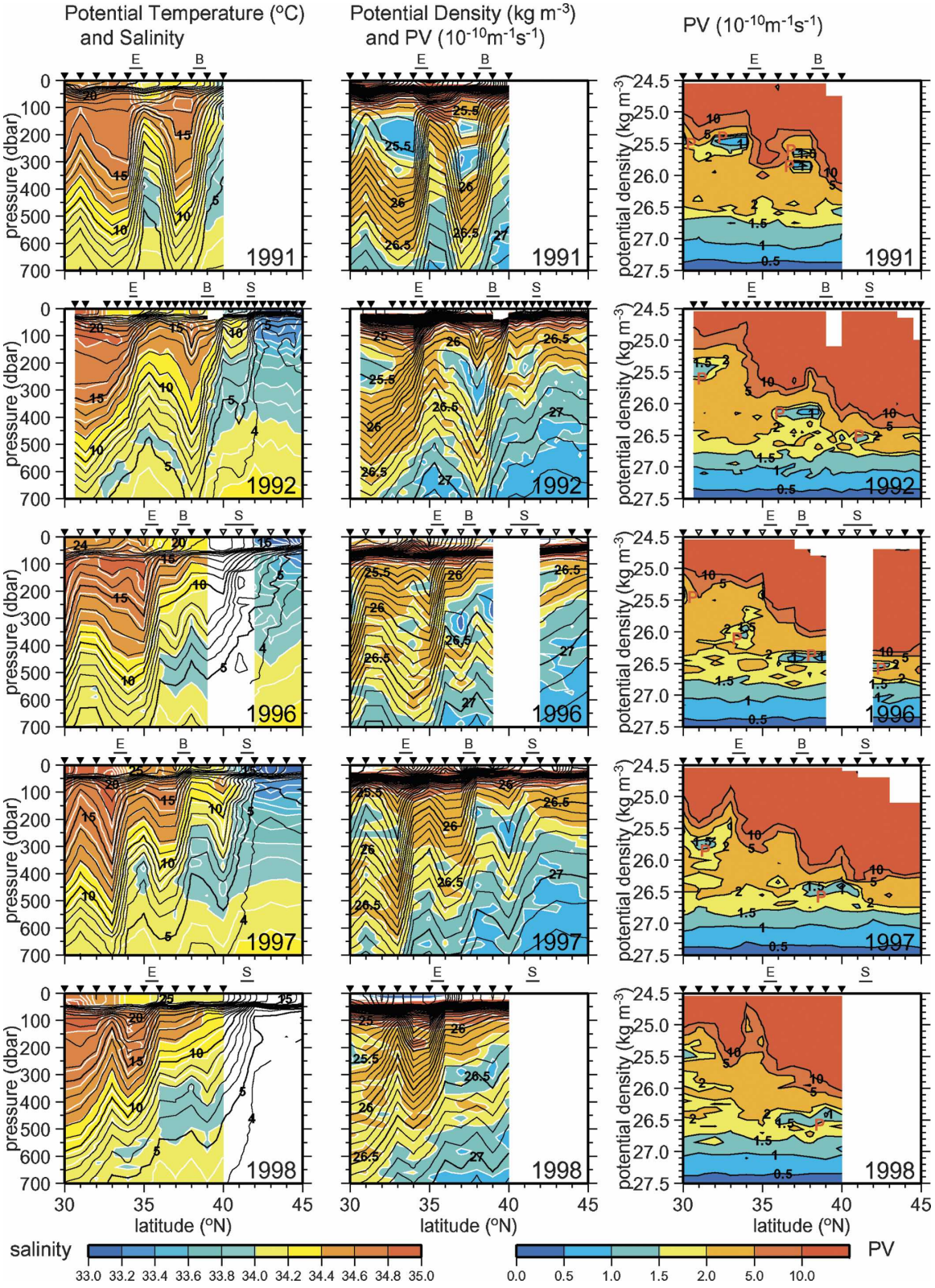

FIG. 3. Distributions in summer, otherwise following Fig. 2.

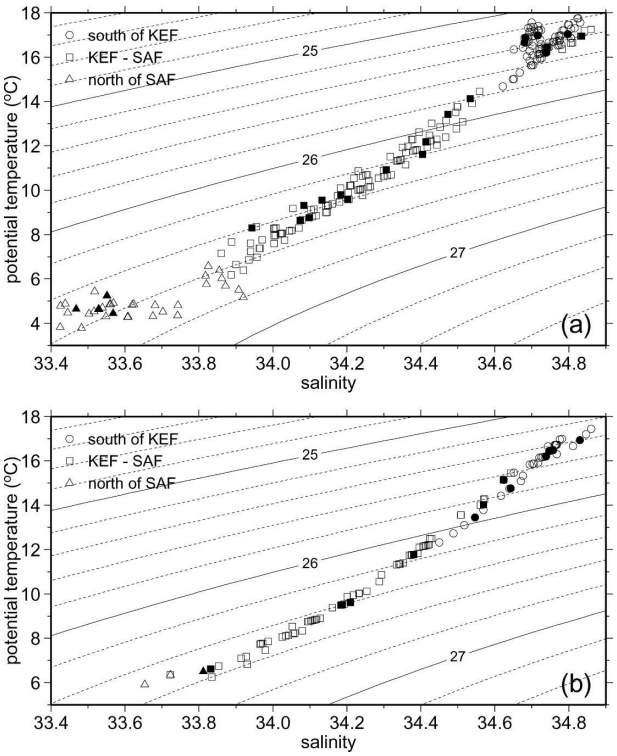

FIG. 4. Potential temperature–salinity relations for pycnostads south of the KEF (circles), between the KEF and the SAF (squares), and north of the SAF (triangles) at 165°E in (a) spring and (b) summer. Black symbols indicate the relations at the core of the pycnostads. Solid and dashed contours denote potential density (kg m^{-3}).

CMW, while the other is STMW. Thus, 12 pycnostads in the spring sections and seven pycnostads in the summer sections are identified as CMW (Table 3). The CMW pycnostads exist in every observation period.

The temperature and density ranges of the CMW pycnostads identified here (6.2°–14.5°C, 25.75–26.65 kg m^{-3}) are somewhat wider than those presented in previous studies based on climatic data (Nakamura 1996; Suga et al. 1997, 2004). To further compare between the former and the latter, the properties at the core of the CMW pycnostads, which is defined by the PV minimum, are examined. The core is considered the least modified portion of a pycnostad since its formation. Therefore, the original properties of the pycnostad at the time of formation are most likely preserved there while the pycnostad is modified through mixing with surrounding water. The core properties of the CMW pycnostads are in ranges of 6.6°–14.1°C and 25.80–26.55 kg m^{-3} (Fig. 4). These more closely resemble temperature and density ranges of the climatological CMW. Since the CMW pycnostads other than the core parts should be small in volume relative to the core parts, they are not likely to survive in climatologies that are smoothed spatially and temporally.

Also, the temperature and density ranges of the CMW pycnostads identified here are adjacent to those of the STMW pycnostads (14.4°–17.8°C, 25.15–25.80 kg m^{-3}) and slightly overlap with them near σ_θ = 25.8 kg m^{-3} (Fig. 4). This boundary isopycnal between CMW and STMW is believed to be correct, because Suga et al. (2004) demonstrated that the isopycnal of σ_θ = 25.8 kg m^{-3} corresponds to both the lowermost isopycnal of STMW and the uppermost isopycnal of CMW, based on climatological isopycnal PV maps.

b. Age of CMW pycnostads

The ages of the CMW pycnostads are deduced from AOU. A similar analysis was performed by Suga et al. (1989) and Suga and Hanawa (1990) for STMW pycnostads near the northwestern corner of the subtropical gyre. We first examine how the AOU values at the core of the eight STMW pycnostads in the spring 165°E sections and the six STMW pycnostads in the summer sections depend on the time of year (Fig. 5a). The AOU is 5–15 μmol kg^{-1} in May and gradually increases in the following months to 26–29 μmol kg^{-1} in September and October. The values in May are comparable to, or slightly higher than, the AOU of the late-winter mixed layer in the STMW formation region southeast of Japan, which is 5–10 μmol kg^{-1} on average, with a standard deviation of about 5 μmol kg^{-1} (Suga and Hanawa 1990). This indicates that the STMW pycnostads at 165°E observed in May are formed in the late winter of the same year (hereinafter referred to as "new"). Moreover, the gradual increase of AOU in the following months implies that the STMW pycnostads in June through October are also new.

The difference among the AOU values in each month is due partly to the degree of dissipation among the STMW pycnostads and partly to how well the discrete dissolved-oxygen data from Niskin bottles resolve vertical AOU minima associated with the cores of STMW pycnostads. When we look at the lowest AOU value for each month that is most unlikely to be affected by such dissipation or discrete sampling, it increases roughly at a rate of 25 μmol kg^{-1} yr^{-1}, which corresponds to the rate obtained by Suga et al. (1989) for STMW observed in a repeat section along 137°E. It should be mentioned that these STMW pycnostads are not considered to be formed in the late winter of the previous year. If they were formed in the previous year, those in the spring sections would have an AOU of about 35 μmol kg^{-1} at the core, and those in the summer sections, about 45 μmol kg^{-1}, assuming an oxygen utilization rate of 25 μmol kg^{-1} yr^{-1} (Suga et al. 1989).

TABLE 2. Locations relative to the fronts (location), number, potential temperature (θ), salinity (S), potential density (σ_θ), and water types (type) of pycnostads at 165°E in (a) spring and (b) summer.

(a)

Location	No.	θ (°C)	S	σ_θ (kg m^{-3})	Type
South of KEF	7	14.7–17.8	34.62–34.83	25.15–25.75	STMW
KEF–SAF	1	16.4–17.2	34.78–34.86	25.35–25.50	STMW
	12	6.2–14.5	33.86–34.56	25.75–26.65	CMW
North of SAF	4	3.8–6.6	33.42–33.91	26.45–26.80	(Subarctic)

(b)

Location	No.	θ (°C)	S	σ_θ (kg m^{-3})	Type
South of KEF	5	14.4–17.5	34.62–34.86	25.30–25.80	STMW
	1	12.3–13.8	34.45–34.57	25.90–26.10	CMW
KEF–SAF	1	15.2–15.4	34.62–34.64	25.60–25.65	STMW
	6	6.3–14.3	33.72–34.57	25.80–26.60	CMW
North of SAF	1	5.9–6.5	33.65–33.81	26.50–26.55	(Subarctic)

The observed AOU for both spring and summer sections is much lower than that value.

The AOU at the core of the CMW pycnostads (Table 3) increases in a similar manner to the STMW pycnostads, except for a high value of 40 μmol kg^{-1} in May (Fig. 5b). Except for this anomalous value, the AOU is 0–16 μmol kg^{-1} in May and gradually increases in the following months. It is therefore inferred that these CMW pycnostads are also new. The high value of 40 μmol kg^{-1} in May, which corresponds to the CMW pycnostad at 35°–36°N in spring 2000, is higher than the other values in May, by roughly 30 μmol kg^{-1}. This pycnostad is believed to be formed in the late winter of the previous year, assuming that the oxygen utilization rate of 25 μmol kg^{-1} yr^{-1} can also be applied to CMW at 165°E.

Since dissolved oxygen data are not available for the two CMW pycnostads in spring 2001 (Table 3a), their formation time is deduced using a CTD-oxygen profile obtained at 40°N a month later (Fig. 6). At this loca-

TABLE 3. Latitudes (lat), potential density (σ_θ), potential temperature (θ), pressure (p), AOU at the core (AOU), and locations relative to the fronts (location) of CMW pycnostads at 165°E in (a) spring and (b) summer.

(a)

Year	Lat (°N)	σ_θ (kg m^{-3})	θ (°C)	p (dbar)	AOU (μmol kg^{-1})	Location
1993	35–37	26.00–26.25	10.9–12.8	80–372	10	KEF–KBF
1996	38–40	26.30–26.45	9.0–10.1	91–285	9	KBF–SAF
1997	36–37	26.00–26.35	10.2–13.1	113–358	15	KEF–KBF
	38–40	26.35–26.55	7.7–10.1	104–329	11	KBF–SAF
1998	37–41	26.30–26.55	7.4–10.6	141–377	24	KEF–SAF
2000	35–36	26.25–26.35	9.6–10.7	219–462	40	KEF–KBF
	36–37	25.85–26.15	11.5–13.9	75–408	8	KEF–KBF
	39–40	26.25–26.50	7.7–10.7	101–307	16	KBF–SAF
2001	37	25.75–25.85	13.8–14.5	170–327	No data	KEF–KBF
	38–40	26.40–26.65	6.2–9.3	133–422	No data	KBF–SAF
2002	40–41	26.35–26.50	7.2–9.2	92–152	9	KBF–SAF
2003	38–40	26.10–26.40	9.1–12.2	18–307	0	KBF–SAF

(b)

Year	Lat (°N)	σ_θ (kg m^{-3})	θ (°C)	p (dbar)	AOU (μmol kg^{-1})	Location
1991	37–38	25.80–25.90	13.6–14.3	236–370	10	KEF–KBF
1992	36–38.5	26.05–26.25	10.9–12.5	153–396	9	KEF–KBF
	41–41.5	26.50–26.60	6.3–7.8	157–255	31	KBF–SAF
1996	34	25.90–26.10	12.3–13.8	299–420	27	south of KEF
	36–39	26.35–26.50	8.3–10.0	173–376	17	KEF–SAF
1997	38–41	26.35–26.55	6.3–10.1	154–312	32	KBF–SAF
1998	36–40	26.30–26.60	6.8–10.6	179–367	30	KEF–SAF

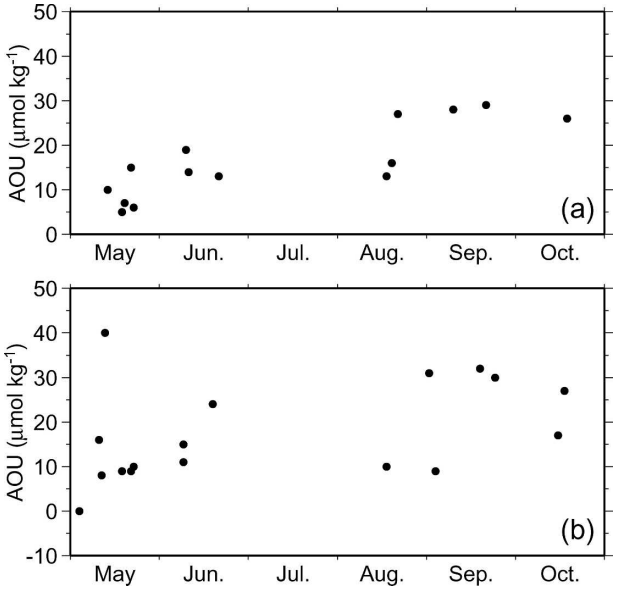

FIG. 5. Plots of AOU at the core of (a) the STMW pycnostads and (b) the CMW pycnostads at 165°E against the observation month.

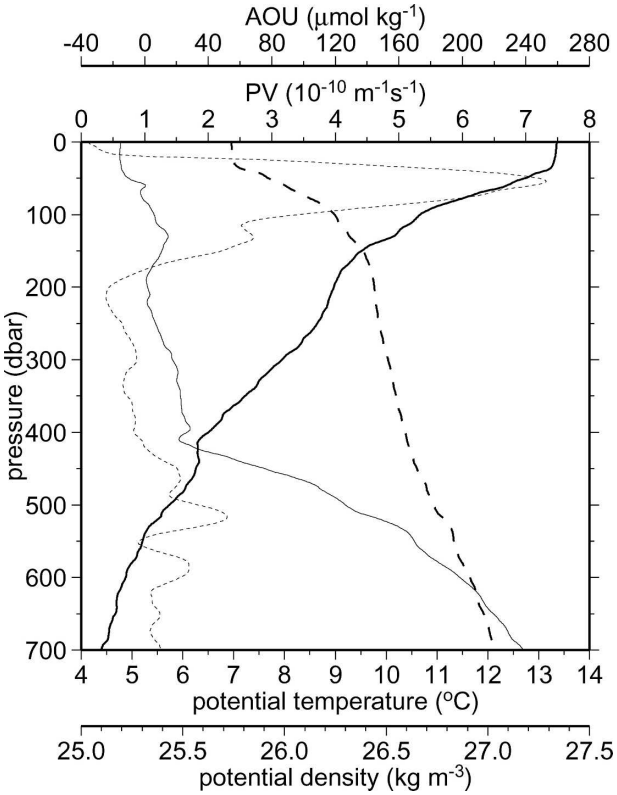

FIG. 6. A vertical profile of potential temperature (thick solid curve), potential density (thick dashed curve), PV (thin dashed curve), and AOU (thin solid curve), obtained at 40.0°N, 165.0°E on 18 Jun 2001 during the R/V *Mirai* MR01-K03 cruise.

tion, a pycnostad of 6.3°–9.3°C and 26.41–26.65 kg m^{-3} is observed between 170 and 440 dbar. It is considered to be identical to the CMW pycnostad at 38°–40°N in the spring section because the properties are almost coincident. It is judged to be new, since it has an AOU of 3 μmol kg^{-1} at the core at 210 dbar. We therefore assume that the two CMW pycnostads in the spring section are new as well. After all, all CMW pycnostads in the spring and summer sections are new, except for one at 35°–36°N in spring 2000 formed in the late winter of the previous year, 1999.

The CMW pycnostad in spring 2003 is located only 20 dbar below the sea surface (Fig. 2), having a particularly low core AOU of 0 μmol kg^{-1} (Table 3a). It has probably been outcropped until just before the observation in early May, that is, until around the end of April. If we assume that the other pycnostads have also been outcropped until around the end of April, we can estimate that the new CMW pycnostads in the spring sections in May and June are aged less than 2 months, and those in the summer sections in August–October are aged 4–6 months. The CMW pycnostad at 35°–36°N in spring 2000 is aged a little over 1 yr.

c. Formation region of CMW pycnostads

Where are these CMW pycnostads formed? The climatological pressure anomaly streamfunction (Zhang and Hogg 1992) relative to 2000 dbar around the 165°E section decreases northward at a rate of 0.5 m^2 s^{-2} per degree latitude (Fig. 1). This gradient is equivalent to an eastward geostrophic flow with a speed of 5 cm s^{-1}. If the new CMW pycnostads at 165°E are advected from their formation regions by this mean flow, those aged 0–2 (4–6) months are to be formed 0–260 (520–780) km west of 165°E, specifically at 162°–165°E (156°–159°E).

The new CMW pycnostads exist at 165°E in every observation period. This implies that CMW is formed between 155° and 165°E every winter. Thus, the CMW formation region extends at least as far west as 155°E, much farther than recognized in our previous study based on climatology.

The CMW pycnostad at 35°–36°N in spring 2000, aged a little over 1 yr, is expected to be formed farther west than the new ones. If the above flow speed is simply applied to this pycnostad, it is to be formed around 147°E. This may occur, because Suga et al. (2004), constructing a winter mixed layer climatology less smoothed than the previous ones, suggested that the CMW formation region possibly extends as far west as 143°E. Unfortunately, the present data at 165°E are insufficient to investigate whether CMW is constantly

formed west of 155°E, since the majority of CMW formed there could be reentrained into the mixed layer and renewed in the next winter, before reaching the 165°E section. Therefore, we leave this problem for a future study, which needs to use synoptic sections in the farther upstream region.

d. Relation between CMW formation region and fronts

The new CMW pycnostads in the spring sections are located in either the interfrontal region between the KEF and the KBF, or between the KBF and the SAF, except for one in spring 1998 (Fig. 2 and Table 3a). The pycnostads between the KEF and the KBF (10.2°–14.5°C, 25.75–26.35 kg m^{-3}) are warmer and lighter than those between the KBF and the SAF (6.2°–12.2°C, 26.10–26.65 kg m^{-3}; Fig. 7). The difference is clearer when we compare the core properties of these pycnostads, which are 11.6°–14.1°C and 25.80–26.20 kg m^{-3} for the southern ones, and 8.3°–10.9°C and 26.25–26.45 kg m^{-3} for the northern ones.

Since these pycnostads are aged less than 2 months and are formed just west of the 165°E section between 162° and 165°E, their locations relative to the fronts have probably been unchanged since their formation. That is, these pycnostads were probably formed in the interfrontal region where they are observed. Thus, two types of CMW, the lighter variety of 25.8–26.2 kg m^{-3} and the denser one of 26.3–26.4 kg m^{-3}, are formed between the KEF and the KBF, and between the KBF and the SAF, respectively. This agrees adequately with the numerical result of Tsujino and Yasuda (2004).

The preferential formation of CMW in these interfrontal regions is explained as follows. These regions, probably corresponding to the "stability gap" south of the SAF (Roden 1970, 1972; Yuan and Talley 1996), are associated with deep winter mixed layers (Suga et al. 2004). The properties of these mixed layers are much more meridionally uniform in the interfrontal regions than within the fronts themselves. Consequently, deep and relatively horizontally uniform mixed layers are formed in each interfrontal region in late winter. They remain as CMW pycnostads in the following seasons, after being capped by the seasonal pycnocline due to the surface warming.

The CMW pycnostad in spring 1998 crosses the KBF, extending over both interfrontal regions (Fig. 2 and Table 3a). Since its properties are of the denser variety, it appears to be formed in the northern interfrontal region and to subsequently intrude into the southern region. The same applies to the pycnostad at 36°–39°N in summer 1996 (Fig. 3 and Table 3b). The pycnostad at 35°–36°N in spring 2000, aged a little over 1 yr, is located between the KEF and the KBF, having properties of the denser variety. It is likely to be formed in the northern interfrontal region and then migrate southward across the KBF. This southward migration to another interfrontal region, where the winter mixed layer density is smaller, must help it to survive the next winter and persist for more than 1 yr. If it stayed in the northern interfrontal region after its formation, it would be largely reentrained into the mixed layer and renewed in the next winter.

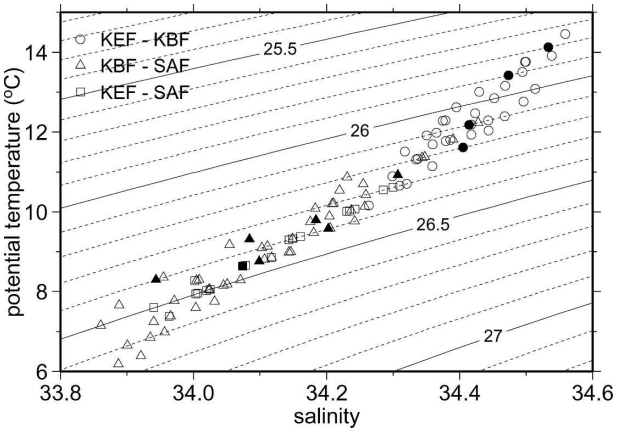

FIG. 7. Potential temperature–salinity relations for the new CMW pycnostads between the KEF and the KBF (circles), between the KBF and the SAF (triangles), and between the KEF and the SAF (squares) at 165°E in spring. Black symbols indicate the relations at the core of the pycnostads. Solid and dashed contours denote potential density (kg m^{-3}).

The pycnostad at 34°N in summer 1996 is located south of the KEF and has properties of the lighter variety. It appears to be formed in the southern interfrontal region and to subsequently migrate southward across the KEF. This case supports Mecking and Warner (2001), who suggested that CMW intrudes southward into the KEF and migrates across it, using distributions of chlorofluorocarbon, PV, and dissolved oxygen in two WHP one-time sections along 165° and 179°E. [The former section is identical to the summer section in 1992 in this study, in which the CMW pycnostad at 36°–38.5°N does not intrude into the KEF at 34°–34.7°N (Fig. 3). This is probably due to the difference in the definitions of CMW and the KEF between Mecking and Warner (2001) and this study.] Thus, some of the CMW pycnostads intrude or migrate southward across the KEF or the KBF as they are advected eastward. This is a form of CMW subduction into the permanent pycnocline.

e. Discussion

While the above analysis has shown that the lighter (denser) variety of CMW is formed in the southern

(northern) interfrontal region between the KEF and the KBF (the KBF and the SAF), the interfrontal region in which CMW is actually formed varies from year to year. The spring and summer 165°E sections indicate that both varieties of CMW pycnostads are formed in winters of 1992, 1996, 1997, 2000, and 2001, while only the lighter (denser) variety is formed in winters of 1991 and 1993 (1998 and 2002). However, if we consider "insignificant" pycnostads of CMW—namely, smaller-scale, low-PV areas of CMW that were neglected in section 4a—the other variety is also formed in most of the latter winters, as clarified below.

In spring 1993, an area of PV lower than 1.5×10^{-10} m^{-1} s^{-1} exists at σ_θ = 26.50 kg m^{-3} at 39°N in the northern interfrontal region (Fig. 2). This is an insignificant pycnostad of the denser variety of CMW, whose extent is limited both meridionally and vertically. It is considered new because it has an AOU of 21 μmol kg^{-1} at the core. Its insignificance may be due to the coarse station spacing in the neighborhood, that is, a lack of observations at 38° and 40°N. In summer 1991, an area of PV less than of 1.5×10^{-10} m^{-1} s^{-1} is seen at σ_θ = 26.55–26.60 kg m^{-3} at 40°N in the northern region, which is also an insignificant pycnostad of the denser variety (Fig. 3). Its insignificance is possibly due to a lack of observations north of 40°N. Since the dissolved oxygen data at 40°N are of poor quality in the depth range of this pycnostad, we cannot judge whether it is new.

In spring 1998, a PV minimum of 1.93×10^{-10} m^{-1} s^{-1}, with an AOU of -1 μmol kg^{-1} (indicating that it is new), exists at 26.00 kg m^{-3} at 37°N in the southern interfrontal region (Fig. 2). This is an insignificant pycnostad of the lighter variety of CMW. Below this exists a significant pycnostad of the denser variety, intruding from the northern interfrontal region. The insignificance of the lighter variety in the southern region may result from mixing with the water coming from the northern region. In spring 2002, a PV minimum of 1.70×10^{-10} m^{-1} s^{-1}, with an AOU of 16 μmol kg^{-1} (new), is seen at 25.95 kg m^{-3} at 37°N in the southern region, which is also an insignificant pycnostad of the lighter variety. In this period, the significant pycnostads of CMW and STMW are thinner than those in the other springs; they are shallower than 250 dbar, whereas those in the other springs are typically located as deep as 300 dbar. Such thinner pycnostads are likely to be dissipated earlier than the average year. After all, if smaller-scale pycnostads are considered, both varieties of CMW are formed in the two interfrontal regions almost every winter, to a varying degree.

The temperature at the core of the two varieties of CMW pycnostads, including insignificant pycnostads,

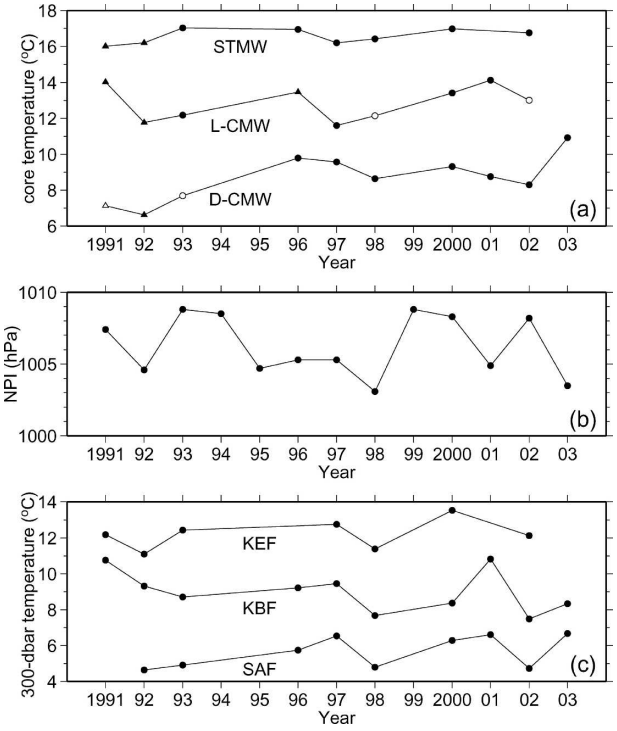

FIG. 8. Time series of (a) potential temperature at the core of pycnostads of STMW and the lighter and denser varieties of CMW (L-CMW, D-CMW) at 165°E, (b) the North Pacific index averaged for Dec–Feb, and (c) potential temperature of the KEF, KBF, and SAF at 300-dbar depth at 165°E. In (a), the temperature for pycnostads in spring is denoted by circles, and that in summer is denoted by triangles; the temperature for significant pycnostads is indicated by black symbols, and that for insignificant pycnostads is indicated by white symbols. In (c), the temperature for the fronts in spring is shown for 1993–2003, and that for the fronts in summer is shown for 1991 and 1992.

changes considerably from year to year (Fig. 8a). The core temperature of the lighter variety fluctuates between 11.6° and 14.1°C, with a mean and standard deviation of 12.9 (±0.9) °C, while that of the denser variety is more variable, between 6.6° and 10.9°C, with 8.8 (±1.2) °C. These contrast with the core temperature of the STMW pycnostads, which changes much less [between 16.0° and 17.0°C, with 16.6 (±0.4) °C].

What causes such large interannual variations of the CMW core temperature? According to Hanawa and Kamada (2001), the core layer temperature of STMW from 1957 to 1996 is positively correlated with the North Pacific index (NPI; Trenberth and Hurrell 1994) on a time scale shorter than 10 yr. The NPI is the area-averaged sea level pressure over the region of 30°–65°N and 160°E–140°W and is a measure of the strength of the Aleutian low. The core temperature of the STMW pycnostads in the 165°E section is positively correlated with the NPI, averaged for December through Feb-

ruary as in Hanawa and Kamada (2001), with a coefficient of 0.48 (Figs. 8a,b). Therefore, the interannual variation of the STMW core temperature is partly due to that of winter surface cooling. However, the core temperature of the lighter and denser varieties of CMW pycnostads bears little correlation with the NPI (coefficients 0.26 and −0.35). This may imply that the properties of CMW pycnostads are strongly influenced by the associated fronts, particularly the KBF, which have high temporal and spatial variability (e.g., Levine and White 1983; Mizuno and White 1983; Sainz-Trapaga et al. 2001).

Consequently, we examine the relation between the core temperature of the two varieties of CMW pycnostads and the temperature of the KEF, KBF, and SAF at 300-dbar depth (Fig. 8c), calculated as the average of the temperature at two stations immediately south and north of these fronts (Table 1). The 300-dbar temperature for each front is negatively correlated with the latitude of the front, with a coefficient of about −0.5 (not shown), so these fronts tend to be colder as they are located northward. The core temperature of the lighter variety of CMW is positively correlated with the 300-dbar temperature of both the KEF and the KBF (coefficients 0.46 and 0.37). The core temperature of the denser variety is highly correlated with the 300-dbar temperature of the SAF (0.77), exceeding the 95% significance level. Thus, it is likely that the properties of the lighter variety of CMW are influenced by both the KEF and the KBF, while those of the denser one are governed primarily by the SAF.

5. Distribution of two types of CMW in the subtropical gyre

How is the differential formation of the two types of CMW reflected in its gyrewide distribution? We examine it by using isopycnal PV distributions constructed from the WHP one-time sections listed in Table 4 (Fig. 9), since the climatological PV maps may not properly represent the CMW distribution, particularly in the upstream region, as mentioned in section 1. Isopycnals of $\sigma_\theta = 26.1$ and 26.4 kg m^{-3} were chosen to represent the lighter and denser varieties of CMW. At 179°E, the low-PV cores of the two varieties lower than 1.5×10^{-10} m^{-1} s^{-1} are meridionally adjacent at 36°–38°N (lighter) and 38°–42°N (denser), as at 165°E, as noted by Mecking and Warner (2001). In the downstream region farther east of the date line, the two varieties diverge considerably. The lighter variety proceeds to 168°–166°W along 30°N, while the denser one is advected along an outer path, to 38°–40°N along 165°W, then to 30°–35°N along 152°W. At 30°N, the two varieties are 1500 km apart.

TABLE 4. WHP one-time sections used to draw Fig. 9.

Section	Nominal location	Period
P02E	30°N	Oct–Nov 1993
P03	24°N	Mar–Jun 1985
P10	149°E	Oct–Nov 1993
P13	165°E (north of 30°N)	Aug–Sep 1992
P13C	165°E (south of 30°N)	Aug–Sep 1991
P14N	179°E	Jul–Sep 1993
P15N	165°W	Sep–Oct 1994
P16N	152°W	Feb–Apr 1991
P16C	152°W	Sep 1991
P17N	135°W (north of 34°N)	May–Jun 1993
P17C	135°W (south of 34°N)	May–Jul 1991

Interestingly, the pathways of both varieties, derived by connecting data points with low PV, cross the contours of climatological pressure anomaly streamfunction and shift to the inner side of the subtropical gyre, toward the downstream. This feature is not caused by the use of the WHP data collected in various years (Table 4), because the same feature is recognized in climatological isopycnal PV maps (see, e.g., Fig. 5 of Suga et al. 2004). The feature occurs possibly because the outer part of CMW is dissipated through mixing with high-PV water on the outer side of the gyre, originated from the northeastern corner of the gyre, while the inner part of CMW is relatively unaffected by dissipation. Alternatively, the inward migration of CMW, which is observed as the southward migration in the 165°E section (section 4d), may be so effective that PV is not conserved along streamlines.

It is also interesting that when the two varieties return to the date line after circulating through the eastern subtropical gyre, they are located at a similar latitude (about 25°N), overlapping each other. This agrees with the result of numerical experiments in Kubokawa and Inui (1999), in which low-PV waters of different densities, formed in different locations near the northern edge of the subtropical gyre, gather in the southwestern part of the gyre after circulating along different paths. The resultant low-PV pool in the model is accompanied by an eastward upper current, resembling the Subtropical Countercurrent in the North Pacific (Uda and Hasunuma 1969), at its southern edge. Based on observations, Aoki et al. (2002) indicated that this low-PV pool is composed not only of CMW, but also of other lighter waters, and is actually accompanied by an eastward current flowing along 18°N (Nitani 1972), which is distinct from the classical Subtropical Countercurrent.

As the WHP sections were observed in various years (Table 4), the CMW circulation presented here needs to be reexamined in a future study, using synoptic data

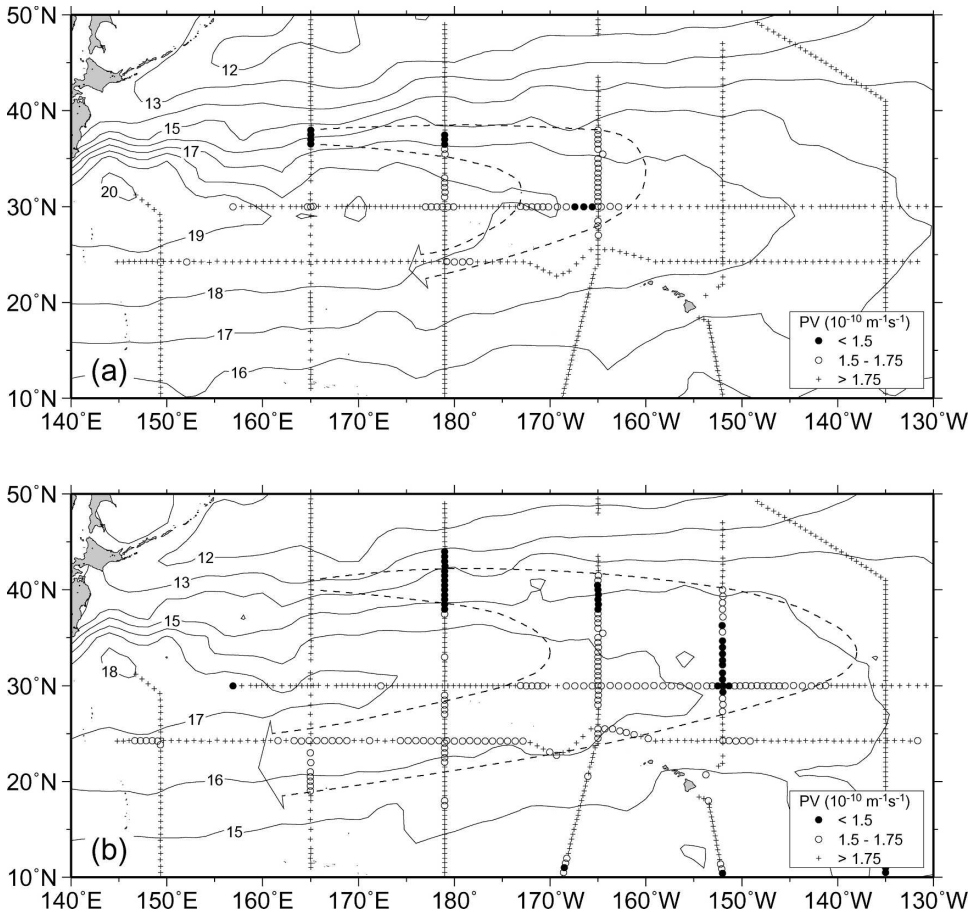

FIG. 9. Distribution of PV on the isopycnals of σ_θ = (a) 26.1 and (b) 26.4 kg m^{-3} at the WHP one-time sections in the North Pacific, indicated by symbols. PV was smoothed isopycnally along each section using a running mean of five hydrographic stations. The dashed arrow roughly encloses a region of PV lower than 1.75×10^{-10} m^{-1} s^{-1}. The solid contours illustrate pressure anomaly streamfunction (m^2 s^{-2}) relative to 2000 dbar on the isopycnals, adapted from Suga et al. (2004).

over the North Pacific obtained in a relatively short period. Data from Argo profiling floats (Argo Science Team 2001) are expected to provide such instantaneous CMW distributions and reveal the temporal variation of CMW on a gyre scale.

6. Summary and discussion

We analyzed CTD and dissolved oxygen data of the 165°E section in springs of 1993, 1996–98, and 2000–03, and summers of 1991, 1992, and 1996–98, to verify the possible westward extension of the CMW formation region and to investigate the relation between the formation region and the thermohaline fronts. The CMW formation region extends at least as far west as 155°E, much farther than recognized in the previous study based on climatic data. It is located in the two interfrontal regions between the KEF and the KBF, and between the KBF and the SAF, where the two types of CMW—namely, the lighter variety of σ_θ = 25.8–26.2 kg m^{-3} and the denser one of 26.3–26.4 kg m^{-3}—are formed. The properties of both varieties exhibit significant year-to-year variations, which seem to be influenced by the KEF and the KBF (lighter variety) and by the SAF (denser variety) that have high temporal and spatial variability.

How the differential formation of CMW is reflected in its gyrewide distribution was further examined using the WHP one-time sections in the North Pacific. The main circulation paths of the two types of CMW diverge east of the date line; the lighter variety is located in the inner part of the eastern subtropical gyre, and the denser variety is located in the outer part. Interestingly, the paths of both varieties depart from the climatological pressure anomaly streamfunction and shift to the inner side of the subtropical gyre, although the reason

is unclear. The gyrewide CMW distribution and its temporal variation, and their relation to the subtropical gyre circulation need to be reexamined quantitatively in a future study, using synoptic data over the subtropical gyre, for example, from Argo profiling floats.

The results of this study demonstrate that the frontal structure around the northern boundary of the subtropical gyre is essential in determining the properties and the gyre-wide distribution of CMW. The existence of KBF is particularly important because it leads to the differential formation. The numerical simulation of Tsujino and Yasuda (2004) was able to reproduce the formation of two types of CMW on each side of the KBF because it successfully reproduced the KBF.

As mentioned in section 1, the western part of the CMW formation region west of 175°E has not been detected in climatological PV maps (e.g., Fig. 1). This is explained as follows. If we suppose a synoptic PV map on a given isopycnal in the CMW density range, PV south (north) of the winter outcrop of the isopycnal must be low (high) because the isopycnal lies in the permanent (seasonal) pycnocline. On the map, the CMW in the western formation region is considered to appear as a zonal band of particularly low PV with a meridional width of a few degrees, located just south of the outcrop. The smoothing process in climatology, however, averages the low PV south of the outcrop and the high PV north. This significantly weakens the low-PV signature of CMW just south of the outcrop, as the smoothing scale is typically as large as the meridional width of the CMW band.

In a future study, we also need to clarify which part of the CMW observed in the 165°E section has been subducted into the permanent pycnocline and which part will be reentrained into the mixed layer in the next winter. Modeling studies have demonstrated that CMW is permanently subducted east of the date line, by crossing a zone of sharp horizontal gradient in the winter mixed layer depth—namely, a mixed layer front—at the eastern end of a region of deep mixed layers (e.g., Kubokawa and Inui 1999; Xie et al. 2000; Tsujino and Yasuda 2004). However, the winter mixed layer climatology of Suga et al. (2004) indicates that such a mixed layer front for CMW does not exist in the real ocean, and CMW is likely to be permanently subducted in a zonally elongated region along the northern boundary of the subtropical gyre between 143°E and 170°W, where the winter mixed layer depth gradually decreases eastward (downstream), while the mixed layer density changes little. Therefore, at least part of the CMW observed in the 165°E section is likely to have been permanently subducted. In addition to this along-stream subduction of CMW, part of the CMW in the 165°E section has also been permanently subducted by migrating southward across the fronts, as explained in section 4d. Thus, the subduction process of CMW is quite complicated and cannot be thoroughly clarified by analyzing one repeat section at 165°E. It needs to be further examined using synoptic data at various locations over the possible CMW formation region.

Acknowledgments. The authors are grateful to the Climate and Marine Department of the Japan Meteorological Agency for supplying the hydrographic data of the 165°E section, including those in 2004 that are unpublished. They also thank Hiroshi Uchida for providing the surface velocity data and Shuichi Watanabe for supplying the *Mirai* hydrographic data. They thank an anonymous reviewer for detailed, insightful, and constructive comments that greatly improved the manuscript. This work was supported by "The Argo Project–Advanced Ocean Observing System" as one of the Millennium Projects of the Japanese Government. Author TS was partly supported by the Japan Society for Promotion of Science [Grant-in-Aid for Scientific Research (B), No. 16340135].

REFERENCES

Akima, H., 1970: A new method of interpolation and smooth curve fitting based on local procedures. *J. Assoc. Comput. Meth.,* **17,** 589–603.

Aoki, Y., T. Suga, and K. Hanawa, 2002: Subsurface subtropical fronts of the North Pacific as inherent boundaries in the ventilated thermocline. *J. Phys. Oceanogr.,* **32,** 2299–2311.

Argo Science Team, 2001: Argo: The global array of profiling floats. *Observing the Oceans in the 21st Century*, C. J. Koblinsky and N. R. Smith, Eds., GODAE Project Office, Bureau of Meteorology, 248–258.

Hanawa, K., and J. Kamada, 2001: Variability of core layer temperature (CLT) of the North Pacific Subtropical Mode Water. *Geophys. Res. Lett.,* **28,** 2229–2232.

JMA, 1997: Data report of oceanographic observations. No. 87, CD-ROM.

——, 1998: Data report of oceanographic observations. No. 88, CD-ROM.

——, 1999: Data report of oceanographic observations. No. 89, CD-ROM.

——, 2001: Data report of oceanographic observations. No. 91, CD-ROM.

——, 2002: Data report of oceanographic and marine meteorological observations. No. 92, CD-ROM.

——, 2003: Data report of oceanographic and marine meteorological observations. No. 93, CD-ROM.

Kawabe, M., and K. Taira, 1998: Water masses and properties at 165°E in the western Pacific. *J. Geophys. Res.,* **103,** 12 941–12 958.

Kubokawa, A., and T. Inui, 1999: Subtropical countercurrent in an idealized ocean GCM. *J. Phys. Oceanogr.,* **29,** 1303–1313.

Levine, E. R., and W. B. White, 1983: Bathymetric influences upon the character of North Pacific fronts, 1976–1980. *J. Geophys. Res.,* **88,** 9617–9625.

Masuzawa, J., 1969: Subtropical Mode Water. *Deep-Sea Res.,* **16,** 463–472.

——, 1972: Water characteristics of the North Pacific central region. *Kuroshio—Its Physical Aspects*, H. Stommel and K. Yoshida, Eds., University of Tokyo Press, 95–127.

Mecking, S., and M. J. Warner, 2001: On the subsurface CFC maxima in the subtropical North Pacific thermocline and their relation to mode waters and oxygen maxima. *J. Geophys. Res.,* **106,** 22 179–22 198.

Mizuno, K., and W. B. White, 1983: Annual and interannual variability in the Kuroshio Current System. *J. Phys. Oceanogr.,* **13,** 1847–1867.

Nakamura, H., 1996: A pycnostad on the bottom of the ventilated portion in the central subtropical North Pacific: Its distribution and formation. *J. Oceanogr.,* **52,** 171–188.

Nitani, H., 1972: Beginning of the Kuroshio. *Kuroshio—Its Physical Aspects*, H. Stommel and K. Yoshida, Eds., University of Tokyo Press, 129–163.

Oka, E., and T. Suga, 2003: Formation region of North Pacific Subtropical Mode Water in the late winter of 2003. *Geophys. Res. Lett.,* **30,** 2205, doi:10.1029/2003GL018581.

Roden, G. I., 1970: Aspects of the mid-Pacific transition zone. *J. Geophys. Res.,* **75,** 1097–1109.

——, 1972: Temperature and salinity fronts at the boundaries of the subarctic-subtropical transition zone in the western Pacific. *J. Geophys. Res.,* **77,** 7175–7187.

Sainz-Trapaga, S., G. J. Goni, and T. Sugimoto, 2001: Identification of the Kuroshio Extension, its bifurcation and northern branch from altimetry and hydrographic data during October 1992–August 1999: Spatial and temporal variability. *Geophys. Res. Lett.,* **28,** 1759–1762.

Suga, T., and K. Hanawa, 1990: The mixed layer climatology in the northwestern part of the North Pacific subtropical gyre and the formation area of Subtropical Mode Water. *J. Mar. Res.,* **48,** 543–566.

——, ——, and Y. Toba, 1989: Subtropical Mode Water in the 137°E section. *J. Phys. Oceanogr.,* **19,** 1605–1618.

——, Y. Takei, and K. Hanawa, 1997: Thermostad distribution in the North Pacific subtropical gyre: The Central Mode Water and the Subtropical Mode Water. *J. Phys. Oceanogr.,* **27,** 140–152.

——, K. Motoki, Y. Aoki, and A. M. Macdonald, 2004: The North Pacific climatology of winter mixed layer and mode waters. *J. Phys. Oceanogr.,* **34,** 3–22.

Trenberth, K. E., and J. W. Hurrell, 1994: Decadal ocean-atmosphere variations in the Pacific. *Climate Dyn.,* **9,** 303–319.

Tsujino, H., and T. Yasuda, 2004: Formation and circulation of mode waters of the North Pacific in a high-resolution GCM. *J. Phys. Oceanogr.,* **34,** 399–415.

Uchida, H., and S. Imawaki, 2003: Eulerian mean surface velocity field derived by combining drifter and satellite altimeter data. *Geophys. Res. Lett.,* **30,** 1229, doi:10.1029/2002GL016445.

Uda, M., and K. Hasunuma, 1969: The eastward subtropical countercurrent in the western North Pacific Ocean. *J. Oceanogr. Soc. Japan,* **25,** 201–210.

Xie, S.-P., T. Kunitani, A. Kubokawa, M. Nonaka, and S. Hosoda, 2000: Interdecadal thermocline variability in the North Pacific for 1958–97: A GCM simulation. *J. Phys. Oceanogr.,* **30,** 2798–2813.

Yuan, X., and L. D. Talley, 1996: The subarctic frontal zone in the North Pacific: Characteristics of frontal structure from climatological data and synoptic surveys. *J. Geophys. Res.,* **101,** 16 491–16 508.

Zhang, H.-M., and N. G. Hogg, 1992: Circulation and water mass balance in the Brazil Basin. *J. Mar. Res.,* **50,** 385–420.

Zhang, R.-X., and K. Hanawa, 1993: Features of the water-mass front in the northwestern North Pacific. *J. Geophys. Res.,* **98,** 967–975.